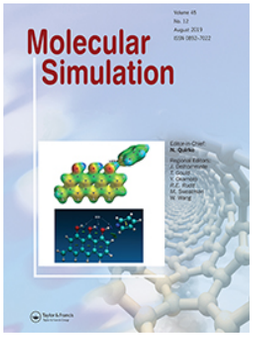

Molecular Simulation

ISSN: 0892-7022 (Print) 1029-0435 (Online) Journal homepage: https://www.tandfonline.com/loi/gmos20

Prediction on elastic properties of Nb-doped Ni systems

Jia Song, Zhibin Gao, Liang Zhang, Wenheng Wu, Beibei He & Lin Lu

To cite this article: Jia Song, Zhibin Gao, Liang Zhang, Wenheng Wu, Beibei He & Lin Lu (2019) Prediction on elastic properties of Nb-doped Ni systems, Molecular Simulation, 45:12, 935-941, DOI: 10.1080/08927022.2019.1614177

To link to this article: https://doi.org/10.1080/08927022.2019.1614177

Published online: 09 May 2019.

MOLECULAR SIMULATION
2019, VOL. 45, NO. 12, 935–941
https://doi.org/10.1080/08927022.2019.1614177

Prediction on elastic properties of Nb-doped Ni systems

Jia Song[a], Zhibin Gao[b], Liang Zhang [a], Wenheng Wu[c], Beibei He[c] and Lin Lu[c]

[a]Shanghai Engineering Research Center of 3D Printing Materials, Shanghai, People's Republic of China; [b]Center for Phononics and Thermal Energy Science, China–EU Joint Center for Nanophononics, Shanghai Key Laboratory of Special Artificial Microstructure Materials and Technology, School of Physics Sciences and Engineering, Tongji University, Shanghai, People's Republic of China; [c]Shanghai Research Institute of Materials, Shanghai, People's Republic of China

ABSTRACT

On the basis of first-principles simulation, the structure, formation enthalpy and mechanical properties (elastic constant, bulk and shear modulus and hardness) of five Nb-doped Ni systems are systematically studied. The calculated equilibrium volume increases with the Nb concentration increasing. The computational elastic constants and formation enthalpy indicate that all Nb-doped Ni systems are mechanically and thermodynamically stable in our research. The hardness of these systems was predicted after the bulk modulus and shear modulus had been accurately calculated. The results show that the hardness increases with the Nb concentration increasing when the Nb concentration was below 4.9%, beyond which the hardness will decrease; this is within the scope of our study.

ARTICLE HISTORY
Received 16 October 2018
Accepted 24 April 2019

KEYWORDS
First-principles simulation; Nb-doped Ni system; formation enthalpy; mechanical property

1. Introduction

Due to the excellent performances such as high-temperature strength, high oxidation resistance and hot corrosion resistance, nickel-based superalloys are currently the key materials in the aerospace field of turbine blades, engine components and combustion chambers [1–3]. Usually, the nickel-based superalloys contain several refractory elements with high melting point and large atomic radii. These elements play a crucial role in improving the properties of nickel-based superalloys. Because of the large difference in electronic structure and atomic radius, different elements play different roles, such as solid solution strengthening, second phase strengthening and grain boundary strengthening [4–6].

In order to meet the development requirements of aerospace, it is necessary to exploit high-performance nickel-based superalloys, especially in terms of good endurance property and structural stability. Many traditional experiments have been done to research the effect of concentration of refractory elements on the nickel-based superalloys. Pröbstle et al. investigated five different Rhenium-free derivatives of CMSX−4 with varying contents of Titanium (Ti) and Tungsten (W). It was found that the concentration of Ti and W resulted in more solid solution strengthener partitioning to the γ phase and significantly improved the creep strength in particular at high temperature and low stress [7]. Wang et al. used a three-dimensional atom probe method to study two kinds of nickel-based superalloys with different contents of Ruthenium (Ru). Their results demonstrated that the addition of Ru element causes more Rhenium (Re) partitioning to the γ' phase and thus the solution strengthening for the γ phase was decreasing [8]. Yeh and Tin applied an electro-thermal mechanical testing to measure the flow stresses of five nickel-based superalloys containing different contents of Re and Ru. The results showed that flow stress significantly increased with the addition of Ru or Re, and the influence of Re on the strengthening the nickel-based superalloy was more than that of Ru [4].

In recent years, as first-principles simulation provides accurate information on energetic and electronic structure from the atomic and electronic levels, many first-principles simulations have been performed to further investigate high-temperature alloy in the aerospace field [9–14]. In this paper, we focus on the effect of strengthening element on the nickel-based superalloys. Geng et al. systematically investigated the site preference of platinum group metals added in the γ'−Ni_3Al by the first-principles total energy calculations. The results suggested that Mo preferred the Al site, and the other platinum group metals (Ru, Rh, Pd, Ir, Os and Pt) preferred the Ni site, in which the capability of element Os was weak [15]. Gong et al. applied density functional theory and Debye−Grüneisen model to study the properties of Ni_3Al with the addition of single alloying elements (W, Re, Mo, Ta and Ru) and co-alloying elements (WRe, WMo, ReMo, WTa, ReTa, WRu and ReRu). It was found that single alloy elements had enhanced effect on mechanical and thermodynamic properties of Ni_3Al, where the effect of W and Re was similar. For the co-alloying elements, there were no distinct synergistic but simple combined strengthening effects on Ni_3Al [16]. Zhao et al. investigated the influence of vacancy on the site preferences of alloying elements Re, Mo, Ta and Cr at the γ/γ' interface in nickel-based superalloys by density functional theory. The calculated results showed that the most preferable substitution sites of alloying elements could not be changed by a Ni vacancy on the (001)γ' plane, except Cr element, and the alloying elements at Al site in γ' enhanced the interfacial bonding strength of the γ/γ' interface, among which the strengthening effect of Re was the best [17].

CONTACT Liang Zhang lzhang0126@hotmail.com

Although many solid-solution strengthening elements, such as Ru, Rh, Pd, Ir, Os, Re, Mo, Ta, Cr and Pt, have been researched by first-principles simulations, there are few studies about Nb element which can improve solid-solution strengthening effect of the γ matrix phase (Ni crystal). In order to reveal the influence of Nb on the γ matrix phase from the atomic and electronic perspective, Ni system doping with Nb element in five different concentrations is systematically investigated by first-principles simulations. The elastic constant and modulus are first calculated to study the effects of the Nb content on the mechanical properties of the above five Ni systems. In addition, with the aid of Pugh's modulus ratio, the hardness of these systems will be predicted after the bulk modulus and spear modulus are accurately calculated. Finally, the Total Density of States (TDOS) and the Partial Density of States (PDOS) of Nb in all systems are investigated.

2. Methodology

2.1. Density functional theory calculations

All spin-polarised DFT calculations were performed with the Vienna Ab-Initio Simulation Package [18–20]. The exchange-correction energy of electron was included via the generalised-gradient approximation using the Perdew–Burke–Ernzerhof functional [21,22]. And the ion–electron interaction was treated with projector augmented wave approach [23]. The electronic wave functions were expanded using the plane wave base functions with a cut-off energy of 500 eV [24]. The energy convergence criterion of the electronic self-consistency was set to 10^{-5} eV per atom, and the force convergence criterion was 10^{-2} eV/Å per atom. Valence electrons used in this study were Ni ($3p^6 4s^2 3d^8$) and Nb ($4p^6 5s^1 4d^4$).

In this study, five different Nb-doped Ni systems were studied: Ni107Nb1, Ni71Nb1, Ni47Nb1, Ni31Nb1 and Ni23Nb1. These supercells were generated through enlarging a Ni cell that contained 4 atoms by $3\times3\times3$, $3\times3\times2$, $2\times2\times3$, $2\times2\times2$ and $3\times2\times1$ with one of the Ni atoms substituted by Nb. Due to the different multiples in the three directions, the Ni71Nb1 (Ni47Nb1) and Ni23Nb1 were tetragonal crystal and orthorhombic crystal, respectively. But, with same multiples in three directions, supercells (Ni107Nb1 and Ni32Nb1) were still cubic crystal. The structure diagram of Ni31Nb1 was used as an example and shown in Figure 1. The Brillouin–zone integration of these systems was conducted using Monkhorst–Pack grids with $2\times2\times2$, $3\times3\times4$, $4\times4\times6$, $8\times8\times8$ and $4\times6\times12$, respectively.

Once the structural optimisation of Nb–doped Ni systems, fcc Ni crystal and Nb crystals was completed, the ground state total energies of these systems would be obtained by first-principles calculations [25,26]. Then the formation enthalpy ($\Delta H(Ni_mNb_n)$) of Nb-doped Ni system could be calculated by the following formula,

$$\Delta H(Ni_mNb_n) = \frac{E_{total}(Ni_mNb_n) - mE(Ni) - nE(Nb)}{m+n} \quad (1)$$

where $E_{total}(Ni_mNb_n)$ was the total energy of an Ni_mNb_n system, $E(Ni)$ was the total energy of an Ni atom in the pure fcc Ni crystal and $E(Nb)$ was the total energy of an Nb atom in the pure fcc Nb crystal.

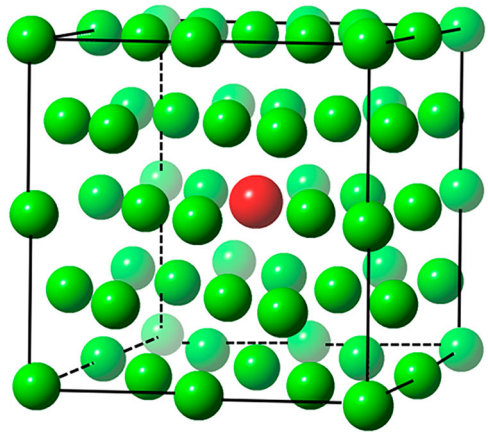

Figure 1. (Colour online) The atomic structure diagram of Ni31Nb1. The red ball represents Nb atom and the rest green balls represent Nb atoms.

2.2. Elastic constants

The elastic constants determined the stiffness of a crystal against an externally applied strain. In the case of small deformation, there was a quadratic dependence of the internal energy on the strain tensor. The elastic constants described the quadratic relationship and were given by [27–31]

$$C_{ijkl} = \frac{1}{V}\left[\frac{\partial^2 E(V,\{\varepsilon_{mn}\})}{\partial_{\varepsilon_{ij}}\partial_{\varepsilon_{kl}}}\right]_{\varepsilon=0} \quad (2)$$

in which, $E(V,\{\varepsilon_{mn}\})$ was the internal energy of the crystal after strain tensor ε_{mn} applied, V was the volume of the unstrained crystal. Generally, the fourth–rank elastic constant C_{ijkl} had no more than 21 independent components. The higher the symmetry of the crystal, the less the number of independent components.

For cubic crystals Ni107Nb1 and Ni31Nb1, there were three distinct, non-vanishing elastic constants, which were C_{11}, C_{12} and C_{44}. The applied strain modes are given in Table 1 [32]. The deformation magnitudes ε from −0.016 to 0.016 in the step of 0.004 were used in the first and second strain modes, and ε from −0.04 to 0.04 in the step of 0.01 were applied in the third strain mode. In the case of orthorhombic crystal Ni23Nb1, nine independent components of elastic constants were C_{11}, C_{22}, C_{33}, C_{12}, C_{13}, C_{23}, C_{44}, C_{55} and C_{66}. The applied strain modes are listed in Table 2 [32]. The deformation magnitudes ε from −0.016 to 0.016 in the step of 0.004 were used in the nine strain modes. For tetragonal crystals Ni71Nb1 and Ni47Nb1, there were six independent components of elastic constants, which were C_{11}, C_{33}, C_{12}, C_{13}, C_{44} and C_{66}. The

Table 1. Parameterisations of the three strain modes used to calculate the three elastic constants of cubic Ni107Nb1 and Ni31Nb1.

Strain *I*	Parameters (unlisted $\varepsilon_i = 0$)	$\Delta E/V_0$ to $O(\gamma^2)$
1	$\varepsilon_1 = \varepsilon_2 = \gamma$, $\varepsilon_3 = (1+\gamma)^{-2}-1$	$3(C_{11} - C_{12})\gamma^2$
2	$\varepsilon_1 = \varepsilon_2 = \varepsilon_3 = \gamma$	$\frac{3}{2}(C_{11} + 2C_{12})\gamma^2$
3	$\varepsilon_6 = 2\gamma$, $\varepsilon_3 = \gamma^2(4-\gamma^2)^{-1}$	$2C_{44}\gamma^2$

Table 2. Parameterisations of the nine strain modes used to calculate the nine elastic constants of orthorhombic crystal Ni23Nb1.

Strain I	Parameters (unlisted $\varepsilon_i = 0$)	$\Delta E/V_0$ to $O(\gamma^2)$
1	$\varepsilon_1 = \gamma$	$\frac{1}{2}C_{11}\gamma^2$
2	$\varepsilon_2 = \gamma$	$\frac{1}{2}C_{22}\gamma^2$
3	$\varepsilon_3 = \gamma$	$\frac{1}{2}C_{33}\gamma^2$
4	$\varepsilon_1 = 2\gamma$, $\varepsilon_2 = -\gamma$, $\varepsilon_3 = -\gamma$	$\frac{1}{2}(4C_{11} - 4C_{12} - 4C_{13} + C_{22} + 2C_{23} + C_{33})\gamma^2$
5	$\varepsilon_1 = -\gamma$, $\varepsilon_2 = 2\gamma$, $\varepsilon_3 = -\gamma$	$\frac{1}{2}(C_{11} - 4C_{12} + 2C_{13} + 4C_{22} - 4C_{23} + C_{33})\gamma^2$
6	$\varepsilon_1 = -\gamma$, $\varepsilon_2 = -\gamma$, $\varepsilon_3 = 2\gamma$	$\frac{1}{2}(C_{11} + 2C_{12} - 4C_{13} + C_{22} - 4C_{23} + 4C_{33})\gamma^2$
7	$\varepsilon_4 = 2\gamma$	$2C_{44}\gamma^2$
8	$\varepsilon_5 = 2\gamma$	$2C_{55}\gamma^2$
9	$\varepsilon_6 = 2\gamma$	$2C_{66}\gamma^2$

applied strain modes were summarised in Table 3 [32]. The deformation magnitudes ε from −0.016 to 0.016 in the step of 0.004 were used in the six strain modes. All simulated elastic constants were obtained by cubic fitting of energy−strain curves because this method yields the smallest errors compared to quadratic fitting and quartic fitting.

Once the independent elastic constants were accurately calculated, two research works could be done. On the one hand, the mechanical stability of Nb−doped Ni systems could be investigated. For the cubic systems, the mechanical stability restrictions were formulated in terms of the elastic constants as follows.

$$C_{11} > 0,\ C_{44} > 0,\ C_{11} - C_{12} > 0,\ C_{11} + 2C_{12} > 0 \quad (3)$$

For the tetragonal systems, the mechanical stability restrictions were formulated in terms of the elastic constants as follows.

$$\begin{aligned} &C_{11} > 0,\ C_{33} > 0,\ C_{44} > 0,\ C_{66} > 0 \\ &C_{11} - C_{12} > 0,\ C_{11} + C_{33} - 2C_{13} > 0 \\ &2(C_{11} + C_{12}) + C_{33} + 4C_{13} > 0 \end{aligned} \quad (4)$$

For the orthorhombic systems, the mechanical stability restrictions were formulated in terms of the elastic constants as follows.

$$\begin{aligned} &C_{11} > 0,\ C_{22} > 0,\ C_{33} > 0,\ C_{44} > 0,\ C_{55} > 0,\ C_{66} > 0 \\ &C_{11} + C_{22} + C_{33} + 2(C_{12} + C_{13} + C_{23}) > 0 \\ &C_{11} + C_{22} - 2C_{12} > 0,\ C_{11} + C_{33} - 2C_{13} > 0 \\ &C_{22} + C_{33} - 2C_{23} > 0 \end{aligned} \quad (5)$$

Table 3. Parameterisations of the six strain modes used to calculate the six elastic constants of orthorhombic crystal Ni23Nb1.

Strain I	Parameters (unlisted $\varepsilon_i = 0$)	$\Delta E/V_0$ to $O(\gamma^2)$
1	$\varepsilon_1 = 2\gamma$, $\varepsilon_2 = -\gamma$, $\varepsilon_3 = -\gamma$	$\frac{1}{2}(5C_{11} - 4C_{12} - 2C_{13} + C_{33})\gamma^2$
2	$\varepsilon_1 = \gamma$, $\varepsilon_2 = -2\gamma$, $\varepsilon_3 = \gamma$, $\varepsilon_6 = 2\gamma$	$(C_{11} + C_{12} - 4C_{13} + 2C_{33} + 2C_{66})\gamma^2$
3	$\varepsilon_1 = -\gamma$, $\varepsilon_2 = -\gamma$, $\varepsilon_3 = 2\gamma$	$(C_{11} + C_{12} - 4C_{13} + 2C_{33})\gamma^2$
4	$\varepsilon_1 = \gamma$	$\frac{1}{2}C_{11}\gamma^2$
5	$\varepsilon_3 = \gamma$	$\frac{1}{2}C_{33}\gamma^2$
6	$\varepsilon_6 = 2\gamma$	$2C_{66}\gamma^2$

On the other hand, based on elastic constants, the shear modulus G and the bulk modulus B of crystal were obtained by the Voigt−Reuss−Hill approximation [33]. In the case of cubic crystal, the bulk modulus and the shear modulus were given by

$$B_V = \frac{1}{3}(C_{11} + 2C_{12}) \quad (6)$$

and

$$G_V = \frac{1}{5}[(C_{11} - C_{12}) + 3C_{44}] \quad (7)$$

In the case of orthorhombic crystal, the shear modulus and the bulk modulus were given by

$$B_V = \frac{1}{9}[C_{11} + C_{22} + C_{33} + 2(C_{12} + C_{13} + C_{23})] \quad (8)$$

and

$$G_V = \frac{1}{15}[C_{11} + C_{22} + C_{33} + 3(C_{44} + C_{55} + C_{66})] \quad (9)$$

In the case of tetragonal crystal, the shear modulus and the bulk modulus were given by

$$B_V = \frac{1}{9}[2(C_{11} + C_{12}) + C_{33} + 4C_{13}] \quad (10)$$

and

$$G_V = \frac{1}{30}[4C_{11} - 2C_{12} + 2C_{33} - 4C_{13} + 12C_{44} + 6C_{66}] \quad (11)$$

Knowing the shear modulus and the bulk modulus, the hardness of polycrystalline materials was correlated with the product of the squared Pugh's modulus ratio k and the shear modulus G according to the work of Chen et al. [34] The mathematical expression was written as

$$H_V = 2(k^2G)^{0.585} - 3 \quad (12)$$

in which, k was the Pugh's modulus ratio, namely, $k = G/B$.

3. Results and discussion

3.1. Structural optimisation

The free energies of a series of Nb−doped Ni systems are calculated by first−principles simulations, and the equilibrium volumes are optimised by fitting these free energies to four-parameter Birch−Murnaghan equation of state as shown in Figure 2 [35,36]. All curves fitting converge satisfactorily and the fitted equilibrium volume and lattice parameters are summarised in Table 4. It can be found the calculated lattice parameters of cubic Ni crystal (consisting of 4 atoms) at 3.51 Å are in good agreement with experimental value of 3.52 Å [37]. The deviation between experimental and theoretical value is less than 0.28%, so we have the reason to consider that structural optimisation method in this study provides satisfactory lattice parameters. In addition, from Figure 2, it can be seen that the equilibrium volume per atom of Nb−doped Ni systems increases with concentrations of Nb. As the concentrations of Nb increase from 1.46% to 6.44%, the equilibrium volume per atom of these systems increases from 10.80 $Å^3$/atom to

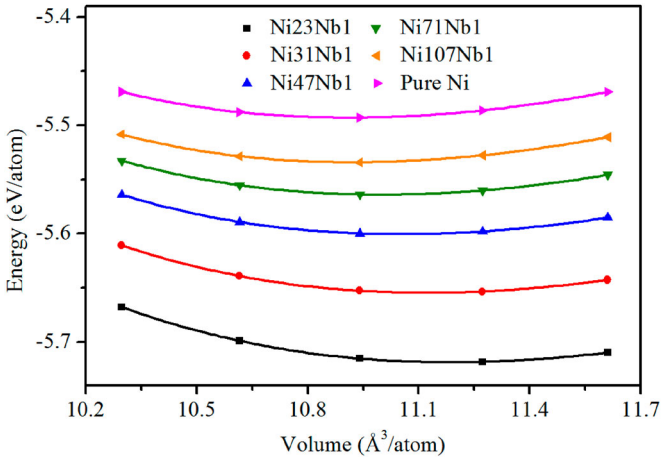

Figure 2. (Colour online) The energy–volume curves of Nb-doped Ni system fitted by four–parameter Birch–Murnaghan equation of state.

Table 4. The lattice parameters, equilibrium volume per atom, bulk modulus, shear modulus and hardness of Nb-doped Ni calculated from first-principles.

System	a Å	b Å	c Å	V_0 Å^3/atom	B_V GPa	G_V GPa	H_V GPa
Ni23Nb1 (Cal.)	10.60	7.08	3.54	11.06	50.7	60.48	24.1
Ni31Nb1 (Cal.)	7.06	7.06	7.06	10.99	67.9	77.9	27.0
Ni47Nb1 (Cal.)	7.04	7.04	10.55	10.91	62.2	69.3	24.0
Ni71Nb1 (Cal.)	10.54	10.54	7.04	10.86	87.9	85.7	23.2
Ni107Nb1 (Cal.)	10.53	10.53	10.53	10.80	133.8	104.7	19.8
Pure Ni (Cal.)	3.51	3.51	3.51	10.79	174.0	119.3	18.1
Pure Ni (Exp.)	3.52	3.52	3.52	10.90	186.0		

11.06 Å^3/atom. The phenomenon can be explained from two aspects. Firstly, the atomic radius of Nb (1.85 Å) is more than that of Ni (1.35 Å), so the substitution of Nb increases the volume of Ni crystal [38]. Secondly, more Ni atoms are replaced by Nb atoms with the increase of Nb content.

According to Equation (1), the formation enthalpies of five Nb−doped Ni systems are calculated and shown in Figure 3. Within the scope of our study, the values of $\Delta H(Ni_mNb_n)$ and Nb content exhibit linear decrease relationship,

$$y = 0.64 - 0.60x \tag{13}$$

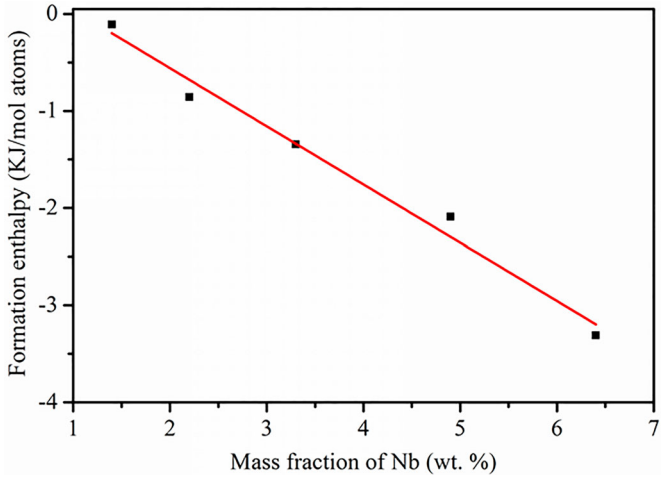

Figure 3. (Colour online) Calculated formation enthalpy for Nb-doped Ni systems. The red line represents a linear relation between formation enthalpy and Nb concentration.

This is because that the interaction between Nb and Ni is gradually weakened with the Nb content decreasing. In addition, the formation enthalpies of examined Nb-doped Ni structures are −3.31, −2.09, −1.34, −0.86 and −0.11 KJ·mol^{-1}·atom^{-1}, which means that these compositions are stable in the ground state.

3.2. Elastic constants and mechanical stability

The elastic constants of Ni crystal summarised in Table 5 are 260.5, 130.7 and 155.5 GPa for C_{11}, C_{12} and C_{44}, respectively, consistent with experimental values of 246.5, 147.3 and 124.7 GPa [37]. These elastic constants also agree with the previous literature values at about 233 GPa for C_{11}, 154 GPa for C_{12} and 128 GPa for C_{44} calculated from embedded−atom −method functions [37]. Therefore, it is concluded that the method of calculated elastic constants in this study is reasonable and can be applied reliably to predict the elastic constants of system of which experimental measurements have not been done.

The array of elastic constants for Nb-doped Ni systems are obtained by using first-principles simulations and summarised in Table 5. Firstly, it is interesting find that the increase of Nb content leads to decrease in all elastic constants values and the reduction of individual elastic constants is different and non-linear, especially for C_{12}. This can attribute that the elastic properties achieved by the first-principles method are extremely susceptible to the parameters and size of atomic models used in computations. What's more, based on these elastic constants, the mechanical stability of Nb-doped Ni systems can be investigated. It can be seen that the elastic constants of cubic systems (pure Ni, Ni31Nb1 and Ni107Nb1) satisfy Equation (3). The elastic constants of tetragonal systems (Ni47Nb1 and Ni71Nb1) fulfil Equation (4). The elastic constants of Ni23Nb1 systems meet Equation (5). To sum up, the five systems in our study are mechanically stable according to elastic constant analysis, which is consistent with formation enthalpy results.

3.3. Modulus and hardness

The bulk modulus, shear modulus and hardness of Nb-doped Ni systems are calculated by using equations (6)–(12) and shown in Table 4. The calculated bulk modulus for pure Ni system is (174 GPa) in good agreement with the experimental value (186 GPa) [39]. In order to interpret our results, the calculated bulk modulus, shear modulus and hardness of Nb-doped Ni systems are plotted in Figure 4. As we can see, the bulk modulus and shear modulus both decrease with the increase of Nb content and can be fitted to a linear relationship,

$$y = a + bx \tag{14}$$

where for the bulk modulus, the parameters a and b are 151.63 GPa and −1833.15 GPa, respectively; for the shear modulus, the a and b are 112.29 GPa and −859.92 GPa, respectively.

According to the intrinsic correlation between hardness and elasticity of materials, the hardness of Nb-doped Ni systems is calculated and listed in Table 4.

Table 5. The elastic constants C_{ij} (unit: GPa) for Nb-doped Ni systems calculated from first-principles.

System	C_{11}	C_{22}	C_{33}	C_{12}	C_{13}	C_{23}	C_{44}	C_{55}	C_{66}
Ni23Nb1 (Cal.)	96.6	99.8	98.0	26.0	28.9	25.9	107.2	97.4	26.6
Ni31Nb1 (Cal.)	90.2			56.7			118.7		
Ni47Nb1 (Cal.)	103.3		93.0	43.4		32.1	123.2		35.9
Ni71Nb1 (Cal.)	169.4		155.2	49.5		40.9	131.0		45.6
Ni107Nb1 (Cal.)	221.9			99.8			140.4		
Pure Ni (Cal.)	260.5			130.7			155.5		
Pure Ni (Cal.)*	233.0			154.0			128.0		
Pure Ni (Exp.)	246.5			147.3			124.7		

*data from previous embedded-atom-method simulations.

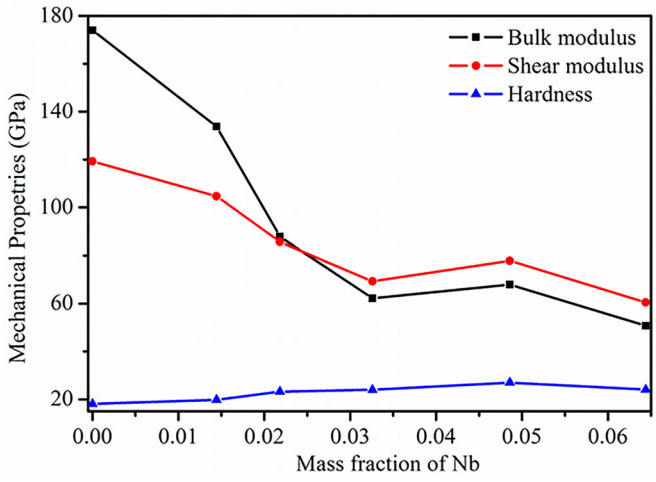

Figure 4. (Colour online) The calculated bulk modulus, shear modulus and hardness of Nb-doped Ni systems varied as a function of Nb concentration.

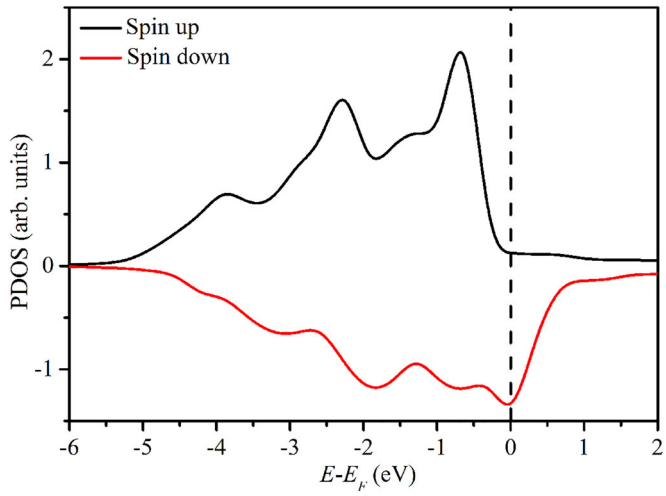

Figure 5. (Colour online) The calculated PDOS for Ni-d orbitals for pure Ni crystal. A vertical dotted line denotes the Fermi energy.

It is interesting note that the hardness of these systems increases as the concentration of Nb increases when the Nb concentration is below 4.9%, beyond which the hardness will decrease; this is within the scope of our study. This phenomenon can be explained from saturability: when the concentration of Nb in the Ni crystal is saturated, the excess Nb element will precipitate as crystal and does not increase the hardness of Nb-doped Ni systems.

3.4. Electronic structure

PDOS on the orbitals for pure Ni are presented in Figure 5. Black line and red line are spin-up and spin-down electrons, respectively, which is in good agreement with former Ref. [40,41] Therefore, it is concluded that the computation of DOS in this study is rational and can be used to analyse the DOS of an unknown system.

In order to better analyse the TDOS of different structural systems, the TDOS is divided by atomic numbers. Figure 6a shows the TDOS per average atom of the five Nb-doped Ni systems and the corresponding PDOS of Nb are portrayed in Figure 6b. Firstly, as shown in Figure 6a, the peak values at −0.68 eV, −2.3 and 1.75 eV demonstrate that Ni and Nb have a strong hybridisation which increases with Nb content increasing. And the difference in TDOS between pure Ni and Nb-doped Ni system explains the nature of vibration of formation enthalpy from atomic perspective. Secondly, the TDOS curves are all mainly located in the energy region from −7 to 10 eV, which indicates that the five compositions in our study possess excellent metallic properties. Thirdly, from the PDOS curves of Nb, it can be seen that contributions of Nb−s orbitals and Nb−p orbitals to the TDOS are almost negligible compared with Nb−d orbitals and the maximum peak of Nb−d orbitals on the right side of Fermi level change with the concentration of Nb element. Comprehensively analysing the curves of TDOS and PDOS, it can be found that the change in the TDOS may be caused by the Nb−d orbitals. In a nutshell, at the atomic level, the substitution of Nb changes the DOS of Ni crystal, thus causing macroscopic change in mechanical properties.

4. Conclusion

In the present work, first−principles simulations are proposed to systematically investigate the structure, formation enthalpy, elastic constants, mechanical properties (bulk modulus, shear modulus and hardness) and electronic structure of five Nb −doped Ni systems.

Firstly, the equilibrium volumes per atoms of the five systems increase as the Nb concentration increases. Secondly, according to the elastic constants results, all the Nb−doped Ni systems are mechanically stable. This can be explained from the perspective of formation enthalpy. The calculated formation enthalpy of all systems is −3.31, −2.09, −1.34, −0.86 and −0.11 KJ·mol^{-1}·atom^{-1}, which means that these compositions are stable in the ground state. Thirdly, the hardness of all

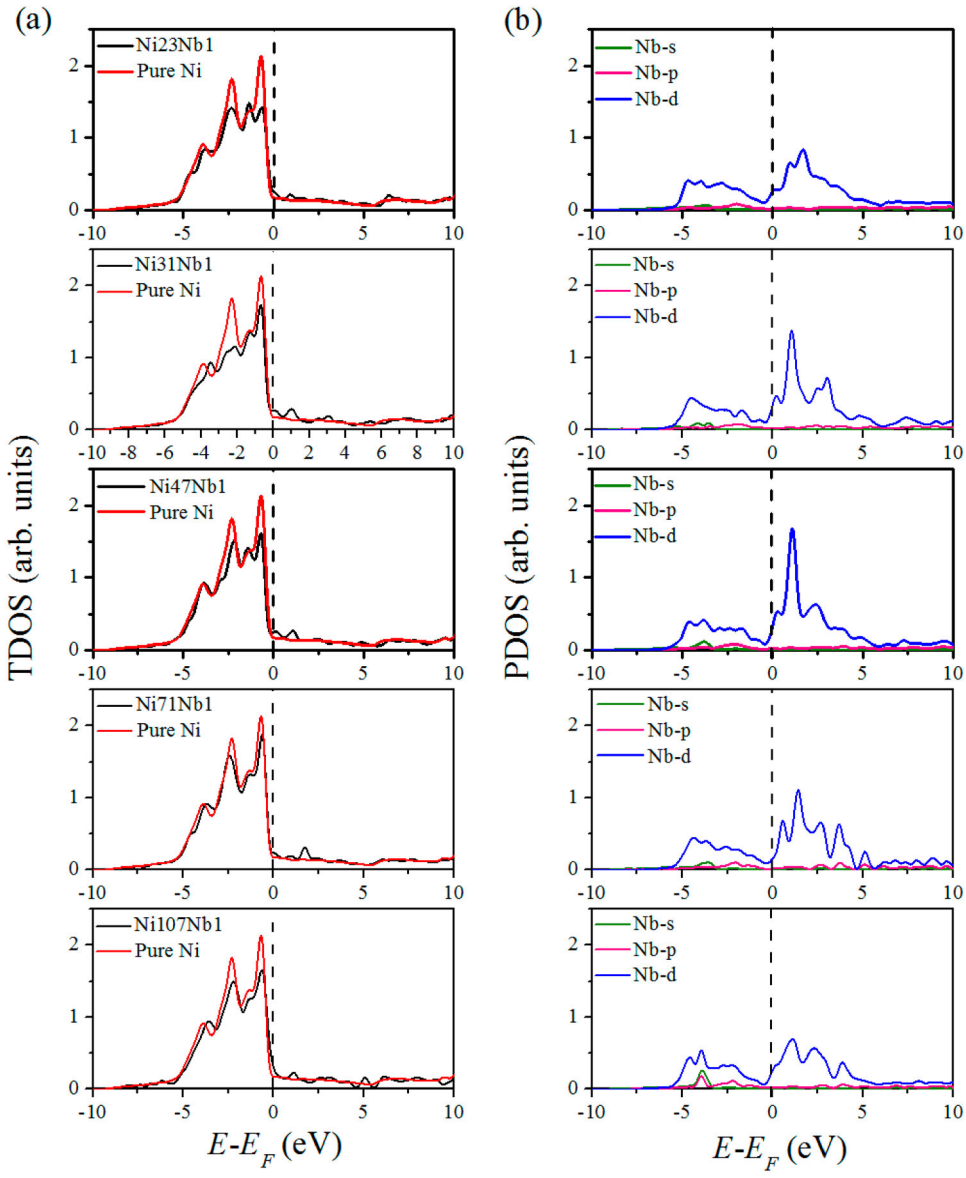

Figure 6. (Colour online) The calculated TDOS per atom (a) and PDOS of Nb (b) in the five Nb-doped systems. A vertical dotted line denotes the Fermi energy.

systems should also be predicted after the bulk modulus and shear modulus have been precisely estimated. The results demonstrate that the hardness increases as the concentration of Nb increases when the Nb concentration is below 4.9%, beyond which the hardness will decrease; this is within the scope of our study. Finally, we further study the electronic structure of these systems, the electron DOS analysis shows that the addition of element Ni will change the TDOS to some extent.

In conclusion, the first-principles is a powerful tool that is helpful in guiding the design and optimisation the composition of Ni–based superalloys.

Disclosure statement

No potential conflict of interest was reported by the authors.

Funding

This work is supported by the project to strengthen industrial development at the grass-roots level is funded by Ministry of Industry and Information Technology (Project Number TC160A310/19), Natural Science Foundation of Shanghai is funded by Shanghai municipal commission of science and technology (Project Number 17ZR1409200), Shanghai Materials and Genomics Engineering Research Institute is funded by Shanghai municipal commission of science and technology (Project Number 16DZ2260605).

ORCID

Liang Zhang http://orcid.org/0000-0003-4253-082X

References

[1] Amato KN, Gaytan SM, Murr LE, et al. Microstructures and mechanical behavior of Inconel 718 fabricated by selective laser melting. Acta Mater. 2012;60(5):2229–2239.
[2] Choi JP, Shin GH, Yang SS, et al. Densification and microstructural investigation of Inconel 718 parts fabricated by selective laser melting. Powder Technol. 2017;310:60–66.
[3] Rong T, Gu DD, Shi QM, et al. Effects of tailored gradient interface on wear properties of WC/inconel 718 composites using selective laser melting. Surf Coat Tech. 2016;307:418–427.

[4] Yeh AC, Tin S. Effects of Ru and Re additions on the high temperature flow stresses of Ni−base single crystal superalloys. Scripta Mater. 2005;52(6):519–524.

[5] Shu DL, Tian SG, Tian N, et al. Influence of Re/Ru on concentration distribution in the γ/γ′ phases of nickel−based single crystal superalloys. Mater Design. 2017;132:198–207.

[6] Wang B, Zhang J, Huang TW, et al. Influence of W, Re, Cr, and Mo on microstructural stability of the third generation Ni−based single crystal superalloys. J MaterRes. 2016;31(21):3381–3389.

[7] Pröbstle M, Neumeier S, Feldner P, et al. Improved creep strength of nickel-base superalloys by optimized γ/γ′ partitioning behavior of solid solution strengthening elements. Mater Sci Eng A. 2016;676:411–420.

[8] Wang XG, Liu JL, Jin T, et al. The effects of ruthenium additions on tensile deformation mechanisms of single crystal superalloys at different temperatures. Mater Design. 2014;63:286–293.

[9] Pan Y, Wen M. The influence of vacancy on the mechanical properties of IrAl coating: first-principles calculations. Thin Solid Films. 2018;664:46–51.

[10] Pan Y, Wang SL, Zhang CM. Ab−initio investigation of structure and mechanical properties of PtAlTM ternary alloy. Vacuum. 2018;151:205–208.

[11] Pan Y. Rual2: structure, electronic and elastic properties from first −principles. Mater Res Bull. 2017;93:56–62.

[12] Pan Y, Jin C. Vacancy−induced mechanical and thermodynamic properties of B2-RuAl. Vacuum. 2017;143:165–168.

[13] Pan Y, Wang P, Zhang CM. Structure, mechanical, electronic and thermodynamic properties of Mo5Si3 from first-principles calculations. Ceram Int. 2018;44(11):12357–12362.

[14] Pan Y, Wang S. Insight into the oxidation mechanism of MoSi2: Ab −initio calculations. Ceram Int. 2018;44(16):19583–19589.

[15] Geng CY, Wang CY, Yu T. Site preference and alloying effect of platinum group metals in γ′−Ni_3Al. Acta Mater. 2004;52 (18):5427–5433.

[16] Gong W, Zhao WY, Miao NH, et al. Strengthening effects of alloying elements W and Re on Ni_3Al: a first−principles study. Comp Mater Sci. 2018;144:23–31.

[17] Zhao WY, Sun ZM, Gong SK. Vacancy mediated alloying strengthening effects on γ/γ′ interface of Ni−based single crystal superalloys: a first-principles study. Acta Mater. 2017;135:25–34.

[18] Kresse G, Hafner J. Ab initio molecular dynamics for liquid metals. Phys Rev B. 1993;47(1):558–561.

[19] Kresse G, Furthmüller J. Efficiency of ab−initio total energy calculations for metals and semiconductors using a plane−wave basis set. J Comput Mater Sci. 1996;6(1):15–50.

[20] Kresse G, Furthmüller J. Efficient iterative schemes for ab initio total −energy calculations using a plane−wave basis set. Phys Rev B. 1996;54(16):11169–11186.

[21] Perdew JP, Burke K, Ernzerhof M. Generalized gradient approximation made simple. Phys Rev Lett. 1996;77(18):3865v3868.

[22] Perdew JP, Burke K. Comparison shopping for a gradient−corrected density functional. Int J Quant Chem. 1996;57(3):309–319.

[23] Blöchl PE. Projector augmented−wave method. Phys Rev B. 1994;50 (24):17953–17979.

[24] Kresse G, Joubert D. From ultrasoft pseudopotentials to the projector augmented−wave method. Phys Rev B. 1999;59(3):1758–1775.

[25] Pan Y. Role of S−S interlayer spacing on the hydrogen storage mechanism of MoS2. Int J Hydrogen Energ. 2018;43(6):3087–3091.

[26] Pan Y, Wen M. Noble metals enhanced catalytic activity of anatase TiO_2 for hydrogen evolution reaction. Int J Hydrogen Energ. 2018;43(49):22055–22063.

[27] Pan Y, Guan WM, Li YQ. Insight into the electronic and mechanical properties of novel TMCrSi ternary silicides from first-principles calculations. Phys Chem Chem Phys. 2018;20(23):15863–15870.

[28] Pan Y, Zhou B. Zrb2: adjusting the phase structure to improve the brittle fracture and electronic properties. Ceram Int. 2017;43 (12):8763–8768.

[29] Pan Y, Wang S, Zhang X, et al. First−principles investigation of new structure, mechanical and electronic properties of Mo−based silicides. Ceram Int. 2018;44(2):1744–1750.

[30] Pan Y. First−principles investigation of the new phases and electrochemical properties of MoSi2 as the electrode materials of lithium ion battery. J Alloy Compd. 2019;779:813–820.

[31] Zhai HC, Li XF, Du JY. First−principles calculations on elasticity and anisotropy of tetragonal tungsten dinitride under pressure. Mater Trans. 2012;53(7):1247–1251.

[32] Beckstein O, Klepeis JE, Hart GLW, et al. First−principles elastic constants and electronic structure of α−Pt_2Si and PtSi. Phys Rev B. 2001;63(13):134112–134123.

[33] Wu ZJ, Zhao EJ, Xiang HP, et al. Crystal structures and elastic properties of superhard IrN_2 and IrN_3 from first principles. Phys Rev B. 2007;76(5):054115–054129.

[34] Chen XQ, Niu HY, Li DZ, et al. Modeling hardness of polycrystalline materials and bulk metallic glasses. Intermetallics. 2011;19(9):1275–1281.

[35] Birch F. Finite elastic strain of cubic crystals. Phys Rev. 1947;71:809–824.

[36] Murnaghan FD. The compressibility of media under extreme pressures. Proc Natl Acad Sci USA. 1994;30:16223–16233.

[37] Foiles SM, Baskes MI, Daw MS. Embedded−atom−method functions for the fcc metals Cu, Ag, Au, Ni, Pd, Pt, and their alloys. Phys Rev B. 1986;33(12):7983–7991.

[38] Slater JC. Atomic radii in crystals. J Chem Phys. 1964;41(10):3199–3204.

[39] Di Marco I, Minár J, Chadov S, et al. Correlation effects in the total energy, the bulk modulus, and the lattice constant of a transition metal: combined local−density approximation and dynamical mean−field theory applied to Ni and Mn. Phys Rev B. 2009;79 (11):115111–115124.

[40] Cinquini F, Delbecq F, Sautet P. A DFT comparative study of carbon adsorption and diffusion on the surface and subsurface of Ni and Ni 3 Pd alloy. Phys Chem Chem Phys. 2009;11(48):11546–11556.

[41] Mohsenzadeh A, Bolton K, Richards T. DFT study of the adsorption and dissociation of water on Ni (111), Ni (110) and Ni (100) surfaces. Surf Sci. 2014;627:1–10.